PERGAMON

Journal of Structural Geology 21 (1999) 653–670

JOURNAL OF STRUCTURAL GEOLOGY

Structures and mechanisms associated with development of a fold in the Cantabrian Zone thrust belt, NW Spain

Gabriel Gutiérrez-Alonso[a,*], Michael R. Gross[b]

[a]*Departamento de Geología, Universidad de Salamanca, 37008 Salamanca, Spain*
[b]*Department of Geology, Florida International University, Miami, FL 33199, USA*

Received 5 January 1998; accepted 22 February 1999

Abstract

A detailed history of progressive fold development based on mesostructural analysis is provided for a metre-scale fold in the Cantabrian fold and thrust belt of northwestern Spain. The well-exposed asymmetric syncline displays a wide variety of structures including extensional faults, thrusts, veins, tectonic stylolites, bedding plane faults, drag folds, and a main limb thrust that transects the entire fold. Important constraints on fold development are provided by the spatial distribution and style of deformation, angular relations, and cross-cutting relations among the structures. Fold mechanisms varied as a function of structural position; while the northwest limb was subjected to pure shear shortening in the form of contractional faults, the southeast limb was bent under tangential longitudinal strain, resulting in a combination of outer-arc extensional faulting in dolostones and simple shear along interbedded shales. Sequential development of the Bárzana fold consisted of; (i) initial flexural slip folding until the southeast limb attained a dip of 60°; (ii) a phase of pressure solution upon locking of bedding plane faults; (iii) shortening accommodated by bed-confined mesofaulting and the propagation of a limb thrust; (iv) unlocking of bedding plane faults and resumption of flexural slip; and (v) propagation of a new limb thrust due to offset of the main thrust by flexural slip. This study demonstrates that a number of very different mechanisms can operate during the course of fold development, and that folding processes and geometries are strongly dependent upon structural position, mechanical stratigraphy, and magnitude of tectonic shortening.

1. Introduction

Folding in unmetamorphosed foreland fold and thrust belts may be accommodated by a number of mechanisms, including flexural slip, tangential longitudinal strain, and internal layer-parallel shortening (e.g. Ramsay, 1967; Geiser and Engelder, 1983; Ramsay and Huber, 1983, 1987; Price and Cosgrove, 1990; Twiss and Moores, 1992). The operative folding mechanism can have a profound effect on fold geometry, the distribution of strain, and the types of structures that develop, all of which may serve to localize ore deposits and/or create structural traps for hydrocarbon reservoirs.

Flexural slip is a mechanism commonly observed in anisotropically layered sedimentary rocks, whereby shear strain is concentrated along discrete horizons. The magnitude of slip depends upon the angle of dip and thickness of the folded layer, and decreases from a maximum at the inflection point to zero in the fold hinge (de Sitter, 1958; Ramsay, 1967; Chapple and Spang, 1974; Tanner, 1989). Competent beds situated between slip horizons often maintain a constant orthogonal thickness, thus resulting in a parallel (Ramsay Class 1B) geometry. Structures that form in response to flexural slip are often related, though not restricted to, simple shear along bedding plane faults, and include dip-slip slickenside lineations, offset bed-normal veins and dikes, rhomb-shaped pull-aparts, asymmetric drag folds, and opposite shear senses on opposing limbs (Ramsay, 1967; Ramsay and Huber, 1987; Tanner, 1989; Becker et al., 1995; Gross et al.,

* Corresponding author.
E-mail address: gabi@gugu.usal.es (G. Gutiérrez-Alonso)

0191-8141/99/$ - see front matter
PII: S0191-8141(99)00055-3

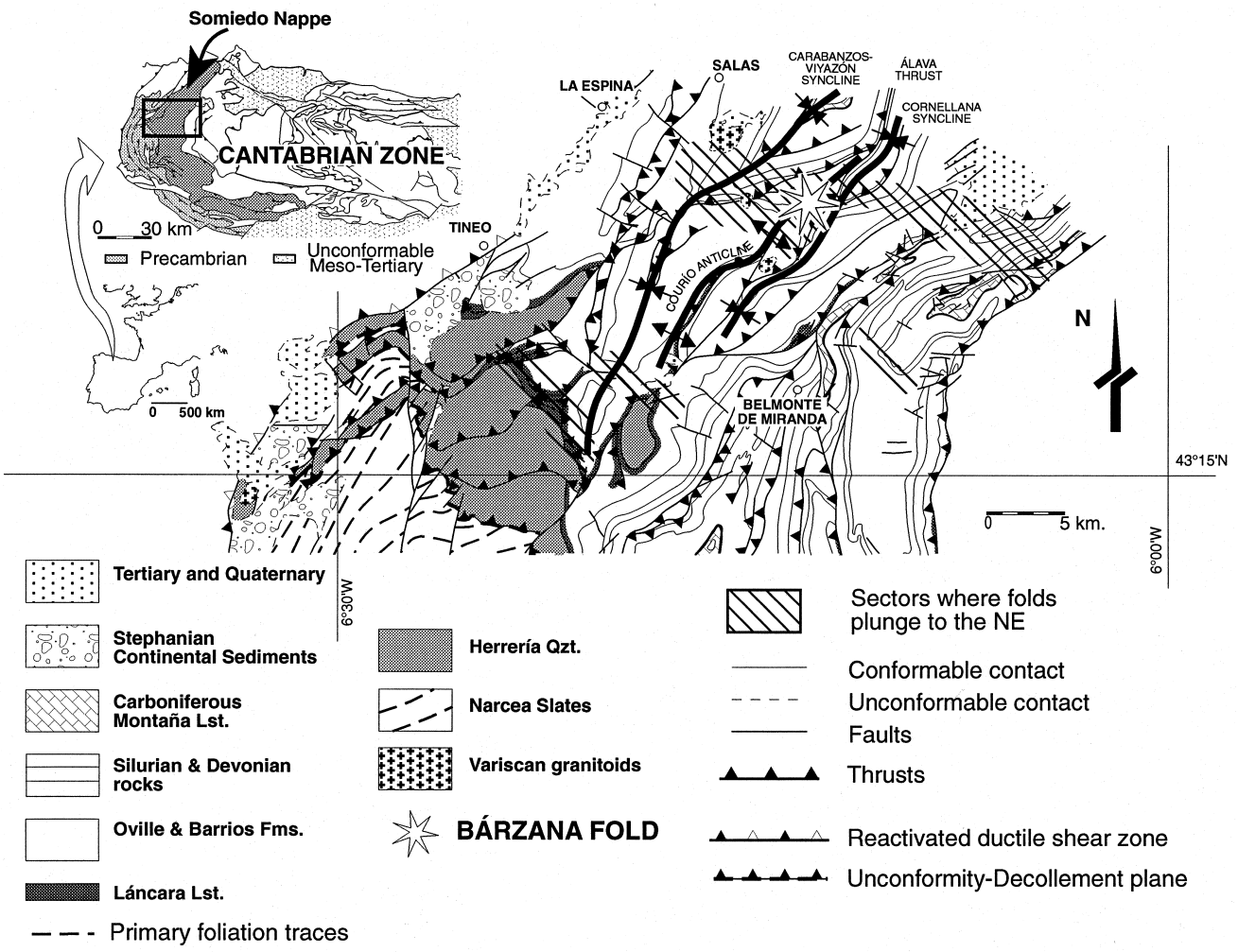

Fig. 1. Geological map of the Cantabrian Zone and the Somiedo Nappe showing location of the Bárzana fold (star) in the study area. Based on mapping of Marcos (1973), Julivert et al. (1977), Crespo Zamorano (1982), Bastida et al. (1984), Heredia (1984), Alonso et al. (1987, 1990), Gutiérrez-Alonso (1987, 1992), Aller et al. (1989), Bastida and Castro, (1989), Bastida and Gutiérrez-Alonso (1989), Suárez et al. (1990).

1997a). Flexural slip along bed boundaries can lead to the development of structures within competent beds, including thrust duplexes, sigmoidal veins, and boudins (Tanner, 1992; Gross et al., 1997a).

Geometrical techniques employed to balance cross-sections in fold and thrust belts typically assume a chevron geometry for fault bend folds (Suppe, 1983), fault propagation folds (Mitra, 1990), and detachment folds (Mitra and Namson, 1989) in order to maintain constant bed thickness, thereby necessitating the operation of the flexural slip mechanism. However, theoretical and laboratory studies demonstrate that flexural slip operates only up to moderate amounts of shear strain and shortening; when limb dips reach ~60°, the slip planes lock, and thus additional fold tightening must be accommodated by other mechanisms (de Sitter, 1958; Ramsay, 1967; Behzadi and Dubey, 1980). This often leads to thinning along limbs and thickening in hinge zones, and a similar (Ramsay Class 2) fold geometry.

The lack of potential slip surfaces in homogeneous competent layers may lead to the development of tangential longitudinal strain (TLS) in response to bending or buckling forces. Unlike flexural slip where simple shear is localized along slip horizons, the magnitude and orientation of the strain ellipse depends upon structural position with respect to a neutral surface (e.g. Ramsay and Huber, 1987). Extension in the outer arc of the layer results in the development of structures such as normal faults and opening-mode veins and joints, whereas thrust faults and cleavage may develop due to inner arc contraction.

Although specific structures and patterns of strain have been linked to individual fold mechanisms as outlined above, constructing a model for progressive fold development is more complex due to the effects of con-

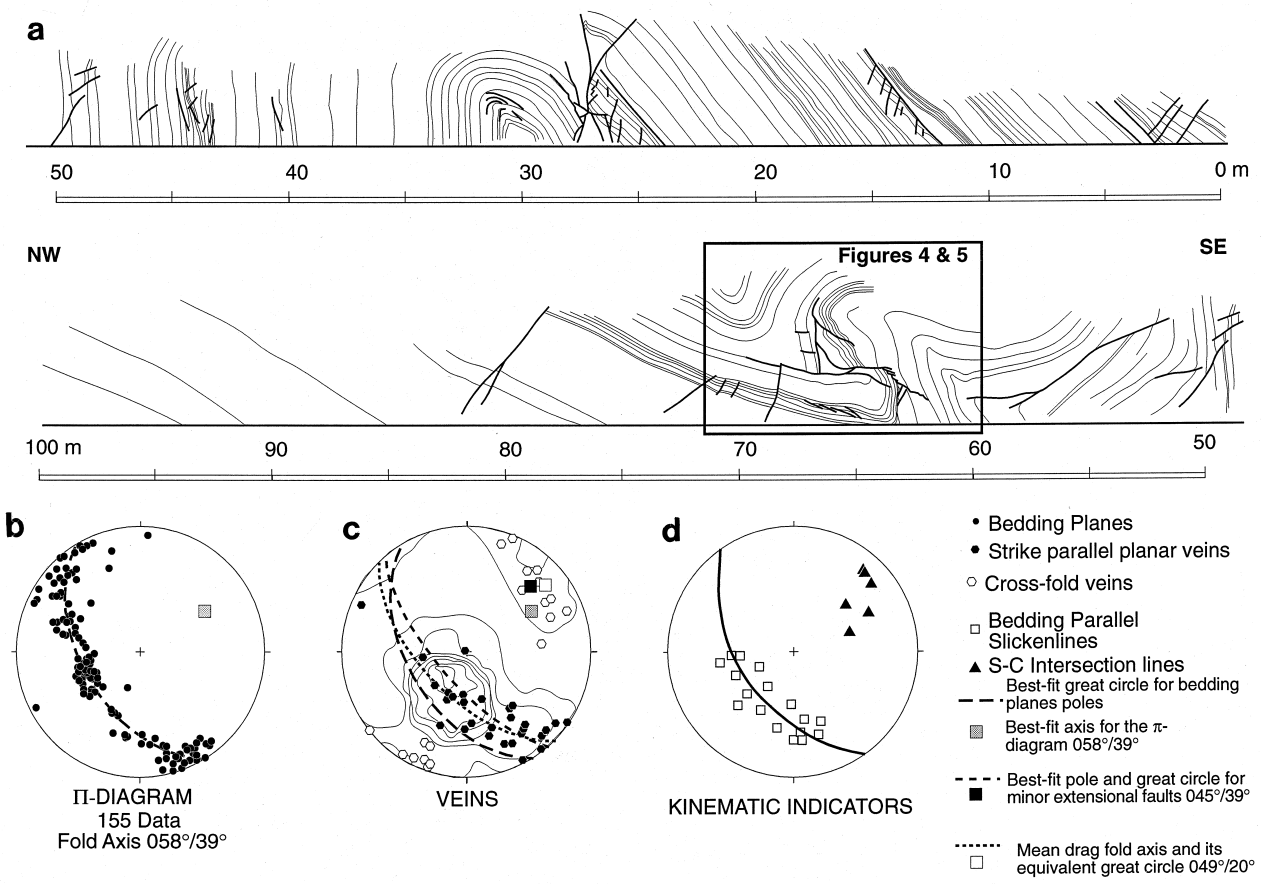

Fig. 2. (a) Sketch of the studied outcrop, with stereoplots of poles to bedding (b), poles to mechanically-confined veins (Kamb contours) (c) and kinematic indicators (d). Detailed structural analysis was performed on the NW-verging syncline located between 70 and 80 m in the section.

trasts in lithology, degree of tectonic development, and structural position. In this study we examine a variety of mesostructures, kinematic indicators, and fold and fault geometries exposed in a metre-scale fold. The excellent exposure and cross-cutting relationships provide the unique opportunity to unravel the progressive deformation of interbedded strata in a fold and thrust belt, and demonstrate that fold mechanisms may indeed vary as a function of mechanical stratigraphy, structural position and inferred temporal development.

2. Geological setting and outcrop overview

The outcrop selected for analysis, referred to as the 'Bárzana Fold', is part of a 100 m long roadcut located 300 m west of the village of Bárzana, between the cities of Oviedo and Cangas del Narcea in Asturias, Spain (Fig. 1). The exposed rocks belong to the Rañeces Group, a 600–700 m thick sequence of bioclastic limestones, dolostones, and shales that were deposited in shallow water marine platforms and tidal flats during the Lower Devonian. The folded carbonates are located above a detachment in the Somiedo Nappe, the rearmost thrust unit of the Cantabrian Zone in the Variscan foreland fold and thrust belt of northwest Spain (Julivert, 1971; Pérez-Estaún et al., 1988, 1991, 1994). A large non-metamorphic structure, the Somiedo Nappe consists of up to 7000 m of mostly stable marine platform Paleozoic sediments imbricated into several major structural units as a result of detachment faulting and out of sequence thrusting (Julivert et al., 1968; Bastida et al., 1984; Heredia, 1984; Gutiérrez-Alonso, 1992, 1996). A structural style characterized by fault propagation folds has intensely folded the rocks in the Somiedo Nappe, resulting in the development of numerous anticline–syncline couples (Alonso et al., 1991). The most prominent folds in the region, which include the Carabanzos–Villazón syncline, the Courio anticline, and the Cornellana syncline, can be traced along strike for tens of kilometres. These folds are characterized by axial traces aligned parallel to the thrusts and mostly subhorizontal fold axes that locally plunge to the northeast in narrow bands, the latter attributed to lateral thrust ramps (Gutiérrez-Alonso, 1987, 1992; Bastida and Castro, 1988; Alonso et al., 1991).

Strata exposed in the roadcut are folded into two

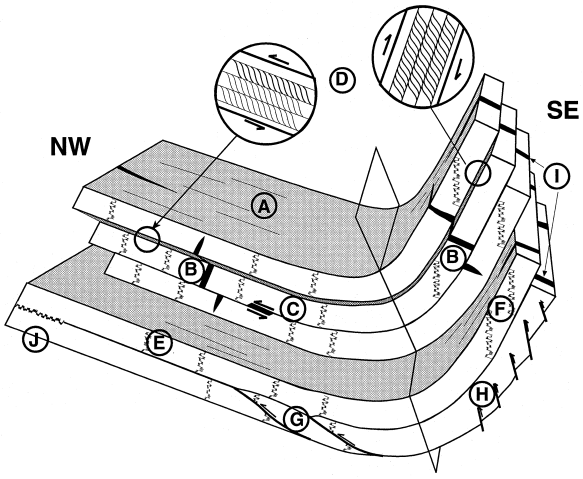

Fig. 3. Schematic representation of mesostructures observed at the Bárzana fold. Note angular relations, evidence for flexural slip, and differences between limbs. Structures are (A) slickenlines, (B) hinge-parallel veins offset by bedding-parallel slip, (C) vein-filled pull-apart graben on bedding surface, (D) *S–C* fabrics in shale beds, (E) bed-normal stylolites on northwest limb, (F) bed-oblique stylolites on southeast limb, (G) thrust faults in dolostone beds on northwest limb, (H) extensional faults (bookshelf geometry) in outer arc of dolostone beds on southeast limb, (I) strike-perpendicular veins, (J) bed-parallel stylolites away from hinge zone.

anticline–syncline pairs (Fig. 2a). The rounded to sub-angular folds display interlimb angles of ~45° and are asymmetric with a northwest vergence and SE-dipping axial surfaces. The most prominent faults are low angle thrusts and bedding-parallel faults with a consistent northwest direction of transport. A π diagram constructed from bedding attitudes measured along the entire length of the roadcut indicates a cylindrical (Ramsay and Huber, 1987) fold train geometry with an axis plunging ~40° to the northeast (Fig. 2b). This calculated fold axis is parallel to the orientations of individual fold hinges measured directly in the outcrop. The plunge of the folds is attributed to the presence of a buried allochthonous lateral ramp, whereas the northwest vergence, opposite to the overall thrust transport direction in the Somiedo Nappe (Fig. 1), may be the result of either backthrusting or backfolding due to underthrusting, all of which are common structures in this sector of the fold belt (Alonso et al., 1991; Gutiérrez-Alonso, 1992). Deformation of the Somiedo Nappe is interpreted as continuous and coaxial throughout the development of the foreland thrust and fold belt (Gutiérrez-Alonso, 1992). Folding at Bárzana is related to development of the Courio Anticline (Fig. 1), which developed in sequence.

Other structural elements observed in abundance throughout the roadcut include extension veins and bedding-parallel fault surfaces. The systematic veins are mechanically-confined to individual beds, as commonly described elsewhere (Narr and Suppe, 1991; Gross et al., 1995), normal to bedding plane surfaces, and group into two main sets. One set of veins is aligned perpendicular to the fold axis (referred to as 'cross-fold' or 'strike-perpendicular' veins) and thus accommodated axis-parallel extension (e.g. Gross and Engelder, 1995). Strike of the second set of veins is aligned parallel to trend of the fold axis ('strike-paral-

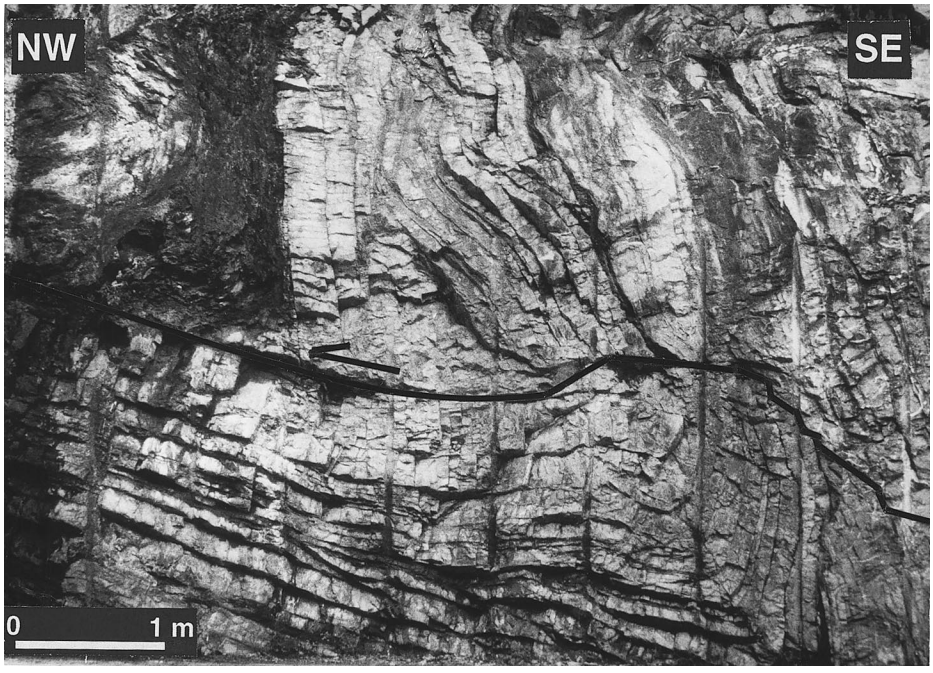

Fig. 4. Photograph of the Bárzana fold in the roadcut from Oviedo to Cangas del Narcea. Note the thrust fault cutting through the southeast synclinal limb that led to hinge collapse. Refer to Fig. 2 for location in cross-section.

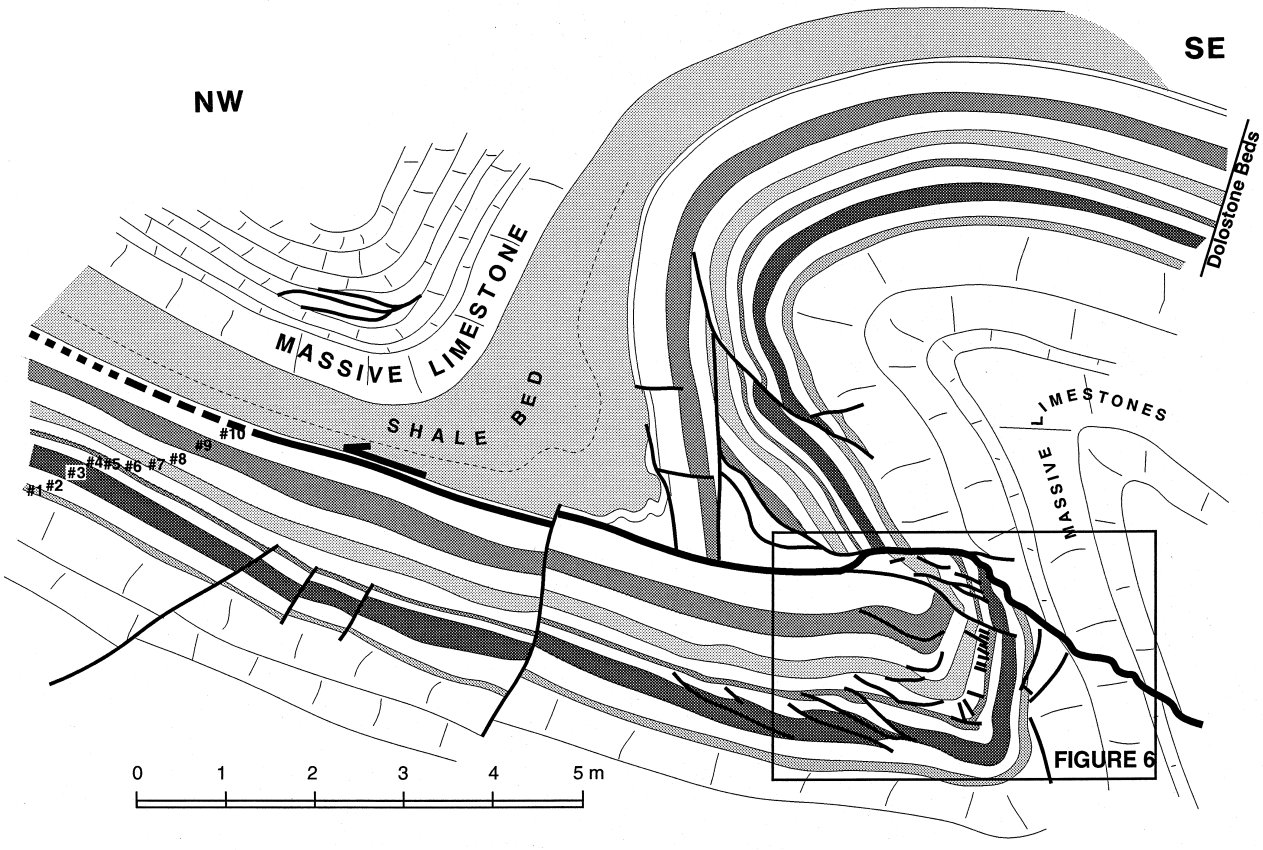

Fig. 5. Corrected down-plunge sketch of the Bárzana fold. Note that ductile shale bed thins along limbs and thickens in the hinge zone, whereas the brittle dolostone unit is characterized by intense faulting in the synclinal hinge zone. Individual dolostone beds are numbered from #1 (stratigraphically oldest) to #10 (youngest).

lel' or 'hinge-parallel' veins), and therefore the amount of dip varies as a function of bedding attitude, though the strike remains approximately the same. For this reason, poles to the strike-parallel veins are scattered in a girdle along the great circle normal to the fold axis (Fig. 2c).

Simple shear motion within shale beds is manifested by a host of kinematic indicators, including prominent dip-slip lineations (i.e. slickenlines) on polished bedding surfaces. The slickenlines fall along the best-fit great circle normal to the fold axis (Fig. 2d), and attest to the operation of the flexural slip mechanism during folding (Ramsay and Huber, 1987; Tanner, 1989). Further evidence for flexural slip includes the alignment of *S*–*C* intersection lineations with the calculated fold axis (Fig. 2d), the offset of strike-parallel veins along bedding faults, and the development of pull-apart veins, all of which indicate the correct out-of-syncline sense of motion with respect to the hinge zone (Fig. 3A–D).

Thin sections of the fine-grained dolostones reveal occasional tectonic stylolite seams and frequent extensional microveins in the strike-parallel orientation. Microscopic fabric is not present, and there is no evidence for homogeneous internal strain. Fossils in the massive limestones underlying and overlying the studied dolostone beds are undistorted, and thus do not reveal internal strain. In contrast, some of the more ductile interbedded shales display an incipient axial-planar cleavage. This behaviour is well recognized not only at the studied outcrop, but also in the surrounding rocks of the Cantabrian Zone.

3. The Bárzana fold: structure and geometry

In an effort to analyse the timing and structural development related to the various mechanisms that operated during folding, we focused on the exceptional suite of mesostructures exposed in the westernmost syncline of the roadcut (Figs. 4 and 5). Of particular interest is a 1.8 m thick package of thinly bedded, buff-coloured micritic dolostone beds bounded below by a ~2 m section of grey bioclastic limestones and above by a ~1 m thick black shale. The overlying shale, which plays a key role in the eventual collapse of the synclinal hinge zone, displays a similar geometry as a result of structural thinning of the limbs and

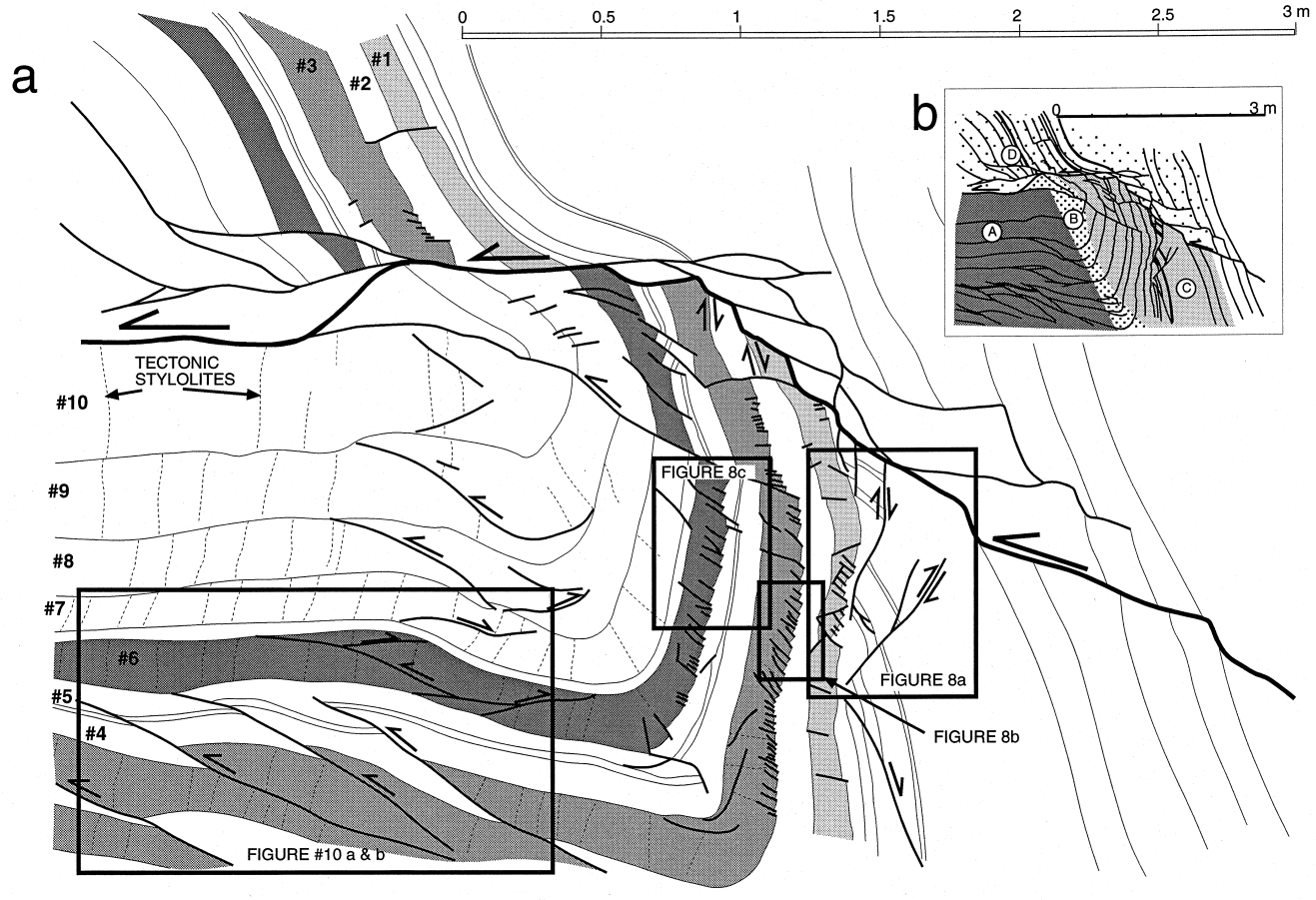

Fig. 6. (a) Detailed outcrop sketch of the Bárzana fold hinge zone. Note thrust faults on northwest limb, outer-arc extensional faults with bookshelf geometry on southeast limb, tectonic stylolites, and staircase geometry of main limb thrust. Boxes refer to photographs presented in Figs. 8 and 10. (b) Inset: division of Bárzana fold into structural domains: (A) moderately dipping northwest limb, (B) hinge zone, (C) subvertical southwest limb beneath main thrust, (D) overturned southeast limb above main thrust.

thickening in the hinge. The steeply dipping to overturned forelimb is transected by a prominent SE-dipping low angle thrust fault, which detaches parallel to bedding upon encountering the thick shale bed in the hinge zone.

Because structural development at Bárzana is a function of many factors, including lithology, structural position, and relative timing, it was necessary to record the data in an accurate and systematic fashion. This was accomplished by detailed photograph-based mapping of the outcrop surface at a 1:10 scale, recording the position and attributes (orientations, kinematics, timing relations) of all mesostructures. In terms of mechanical stratigraphy, the dolostone section consists of ten individual dolostone beds (labelled #1–#10 in Figs. 5 and 6) ranging in thickness from 4.8 cm (bed #5) to 43 cm (bed #10), interbedded with four thin cm-scale shale horizons. The overwhelming majority of mesostructures are mechanically-confined to individual beds. Within dolostones, these structures include thrust faults, extensional faults, and tectonic stylolites, as well as the aforementioned veins. In contrast, the interbedded shales accommodate bedding plane slip and structurally detach packages of dolostone beds from each other. In the absence of intervening shales, dolostone beds are sutured together along bedding-parallel stylolites of diagenetic origin (shown schematically in Fig. 3J), effectively precluding slip along these contacts.

In the following paragraphs we describe the geometry and distribution of the structural elements observed at the Bárzana fold. The fold is divided into four structural domains: a moderately dipping northwest limb, a narrow, rounded hinge zone, the subvertical portion of the southeast limb beneath the main thrust fault, and the overturned portion of the southeast limb above the main thrust (Fig. 6b).

3.1. Tectonic stylolites

Two sets of tectonic stylolites are found in dolostone beds of the Bárzana fold, and are distinguished from each other on the basis of orientation, structural position, and angle with respect to bedding. In all cases

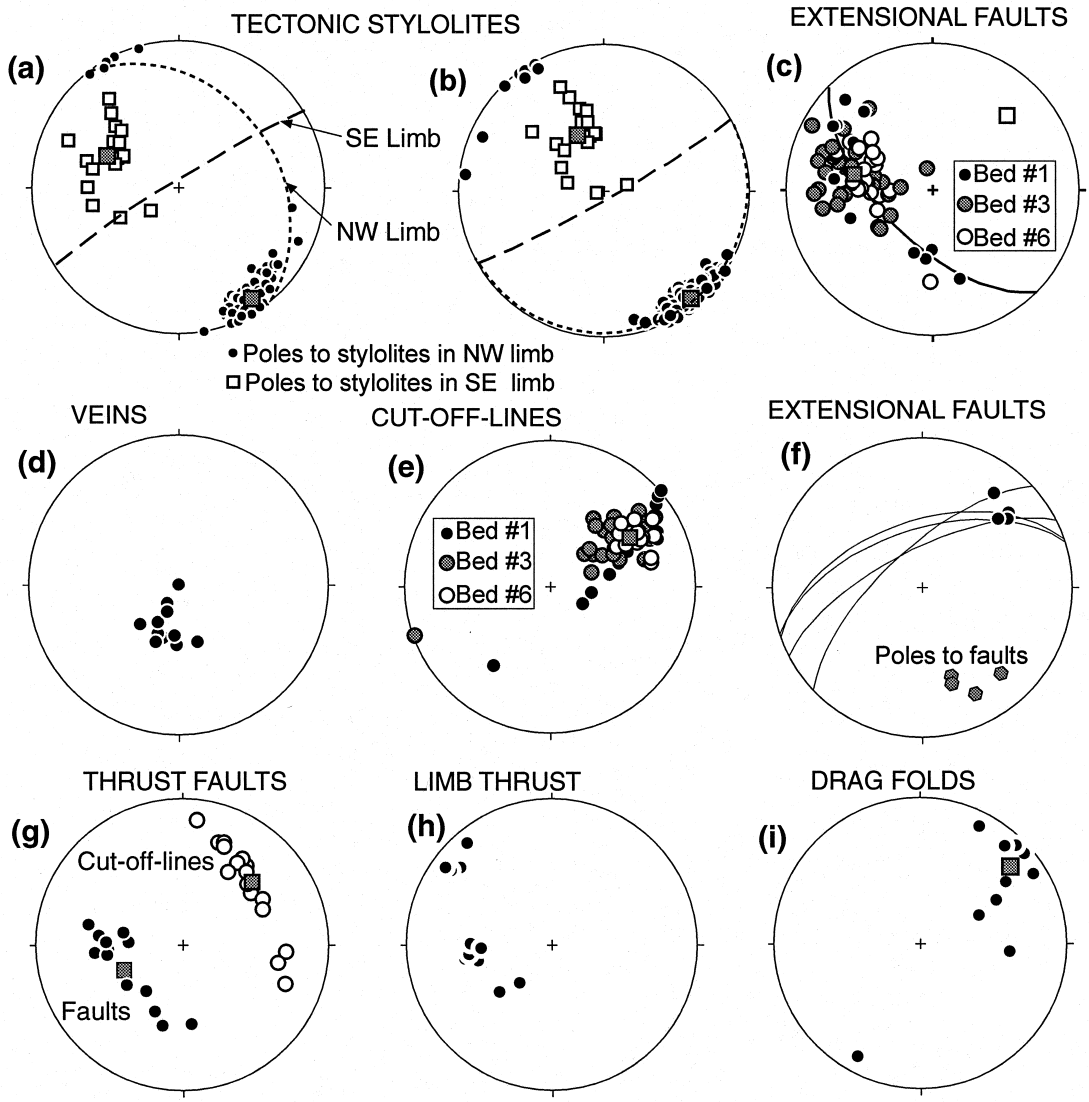

Fig. 7. Lower hemisphere, Schmidt projections of structural features found in the Bárzana Fold. Mean values are represented by grey squares. (a) In situ orientations of poles to tectonic stylolites (mean stylolite pole on northwest limb = 146°/10°; mean stylolite pole on southeast limb = 296°/45°), along with great circles representing general bedding for the two limbs. (b) Plot of poles to tectonic stylolites upon removal of fold plunge (i.e. horizontal fold axis), clearly showing angular relationships between stylolites and limb dip (mean stylolite pole on northwest limb = 141°/06°; mean stylolite pole on southeast limb = 335°/55°). (c) Poles to extensional faults in dolostone beds of the southeast limb. Note the poles cluster along the great circle normal to the fold axis (045°/29°white square). (d) Poles to veins in dolostone bed #1 on southeast limb. (e) Intersection lines between extensional faults and bedding (i.e. cut-off lines) in dolostone beds of southeast limb. Note clustering (grey square, mean = 059°/36°) around fold axis for all three beds. (f) Extensional fault planes (great circles) and cut-off lines (black dots) in massive bioclastic limestones on the southeast limb. (g) Poles to thrust faults (black dots, mean = 245°/54°) and corresponding cut-off lines (white dots, mean = 047°/36°) on northwest limb. White square is fold axis (h) poles to main limb thrust measured at various positions along the fault. Note shallow and steeply dipping segments corresponding to staircase geometry. (i) Drag fold hinges in vicinity of main thrust (mean = 049°/20°).

the stylolite teeth are aligned normal to the pitted solution surface, implying that the axis of maximum shortening during stylolite development was aligned parallel to the pole to the stylolite surface (e.g. Choukroune, 1969; Eyal and Reches, 1983).

Although both sets of tectonic stylolites are mechanically-confined to individual dolostone beds and strike parallel to fold axis trend, the stylolites on the southeast limb are more shallow dipping than those on the northwest limb (Fig. 7a). The angle between mean orientations of the two stylolite populations is 61°. Furthermore, whereas the tectonic stylolites on the northwest limb are perpendicular to bedding (mean angle of 87°), those on the southeast limb are inclined at an average oblique angle of 60° to bedding. This angular relationship is evident from the stereoplots, where for the northwest limb the great circle representing bedding passes through poles to stylo-

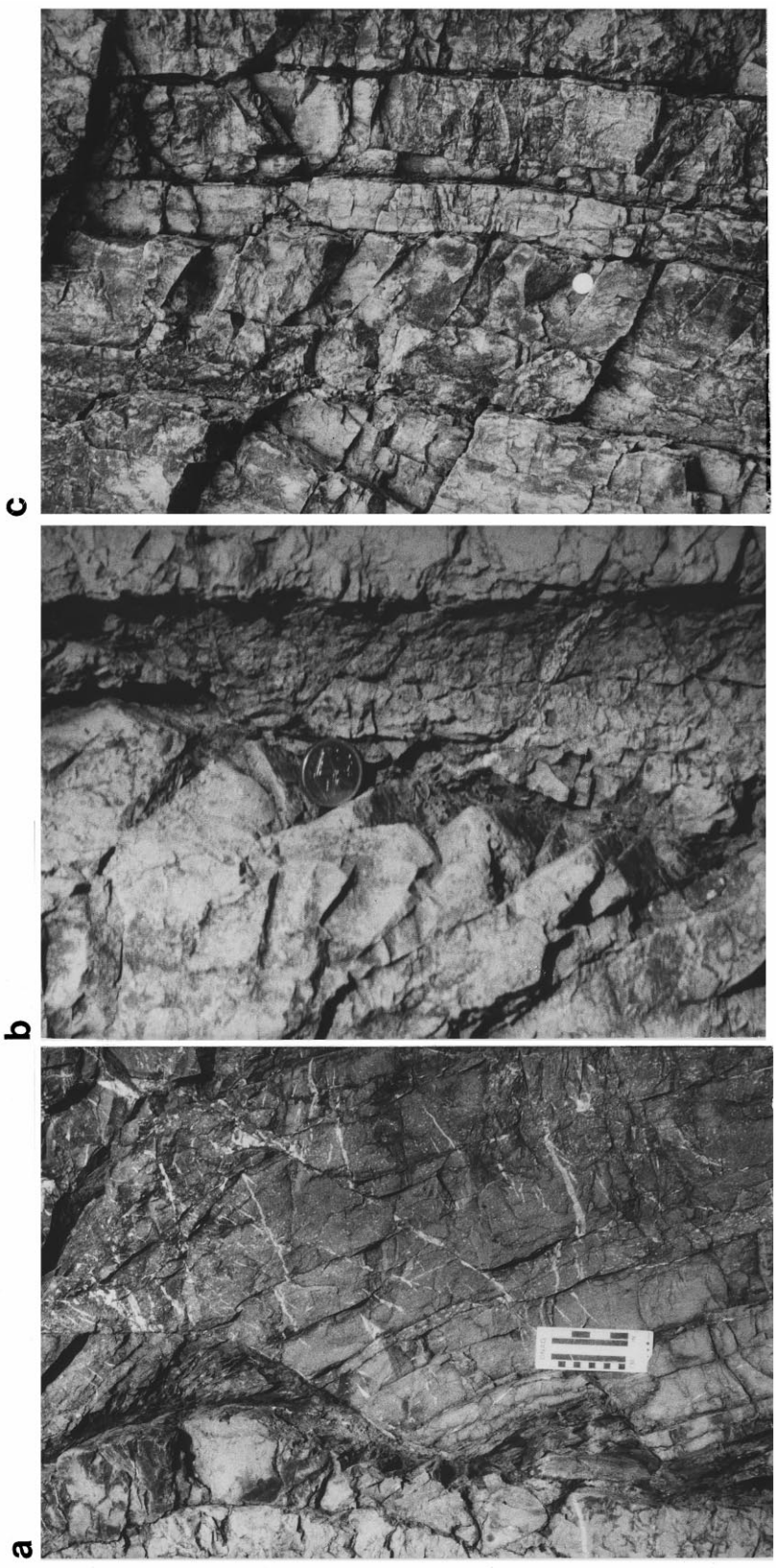

Fig. 8. (a) Photograph of extensional faults and rotated fault blocks in dolostone bed #1 and underlying bioclastic limestones on the southeast limb. Note the triangular-shaped shale pockets along the contact between dolostone and limestone units, and the opposing fault dips in the two lithologies. (b) Photograph of extensional faults in outer arc of dolostone bed #3 on the southeast limb. Note bookshelf geometry implying simple shear along shale contact while dolostone was subjected to tangential longitudinal strain. (c) Photograph of extensional faults in bed #6 of southeast limb. Diameter of coin for (b) and (c) is 17 mm.

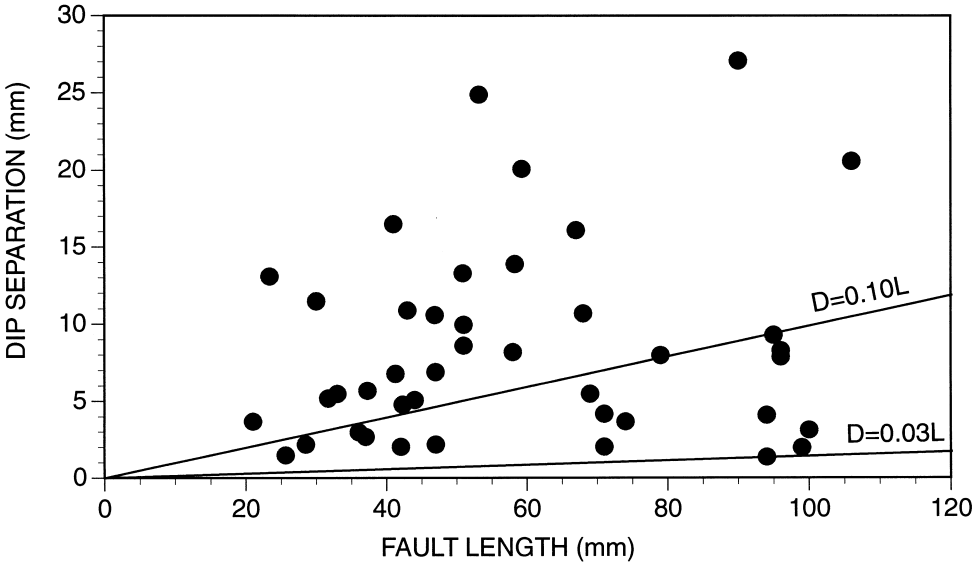

Fig. 9. Plot of dip separation vs length for outer-arc extensional faults with bookshelf geometries in dolostone beds of the southeast limb. Lines represent D–L relationships for small normal faults determined by Schlische et al. (1996) in sandstone ($D = 0.03L$) and by Gross et al. (1997b) in mudstone ($D = 0.10L$). Note the lack of correlation, implying interaction of the faults with the shale detachment.

lites, while for the southeast limb an angle of 30° separates bedding from the mean pole to tectonic stylolites (Fig. 7a and b).

Tectonic stylolites on the northwest limb are relatively consistent in their orientation, as demonstrated by the tight clustering of poles (Fig. 7a). They also exhibit an even spacing within each bed (Merino et al., 1983; Merino, 1992), approximately equal to, or slightly less than bed thickness (Fig. 6). Stylolites on the southeast limb display more scatter in orientation due to the greater amount of bedding curvature, and are less abundant as a consequence of the shorter limb length and subsequent deformation that renders many of them unrecognizable. Amplitudes for stylolite seams range between 1 and 5 mm. Based on stylolite amplitude and spacing we estimate less than 5% shortening due to the pressure solution mechanism.

3.2. Extensional faults

Among the most abundant structural elements found in the Bárzana fold are cm-scale extensional faults whose distribution, both with respect to the hinge zone as well as to depth of propagation within each bed, is critical to understanding the mechanisms that operated during fold development. The faults are exclusively found in the C domain of the steeply dipping southeast limb, and are divided into two main categories—faults within the dolostone section, and faults in the underlying bioclastic limestones. We refer to these faults as 'extensional' rather than 'normal' because they accommodate extension of the beds in the southeast limb, despite their mostly apparent thrust (i.e. upward hanging wall motion) geometry.

Extensional faults in the dolostone section are mechanically-confined and found only in beds #1, #3, and #6 of the southeast limb (Figs. 6, 8, 9 and 10), all of which are bounded at their bases by thin shale detachments. The faults in bed #1 include a combination of several conjugates that extend across the entire bed, as well as a number of smaller, uniformly-oriented SE-dipping faults. Unlike the other two beds, bed #1 also contains carbonate-filled systematic veins aligned normal to the bedding surface and parallel to the fold axis trend (Fig. 7d).

In beds #3 and #6 the extensional faults are more prominent and evenly spaced, though orientations are similar to those in bed #1, with poles to faults clustering along a great circle approximately normal to the fold axis (Fig. 7c). Extensional faults in beds #3 and #6 display the following noteworthy characteristics. First, the overwhelming majority of faults extend from the stratigraphic base of the bed to the middle of the bed. Restriction of faults to the outer arc of these beds implies the presence of a neutral surface and outer-arc extension due to tangential longitudinal strain (TLS). Second, the maximum fault displacement occurs at the contact between underlying shales and decreases to zero at fault tips in the bed centre, implying that faults initiated at the bed boundary and propagated toward the bed centre, further supporting the TLS mechanism. Third, slip along the extensional faults resulted in the creation of bookshelf structures, with a consistent ~23° clockwise rotation of the hanging wall around

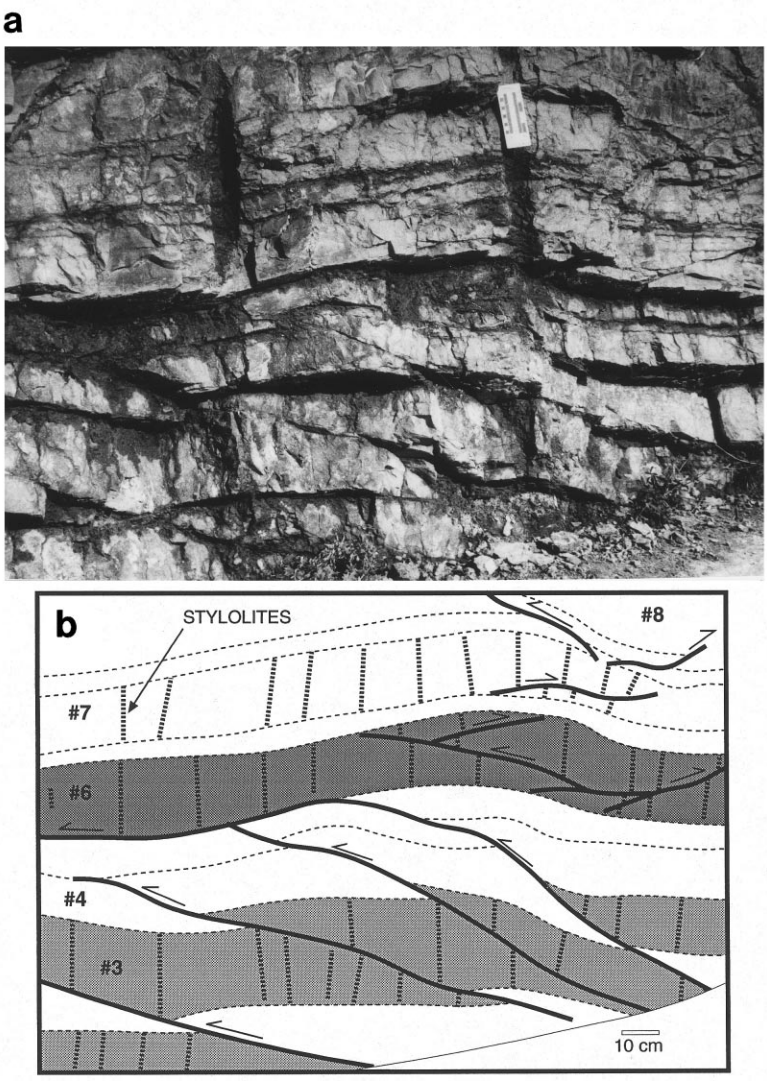

Fig. 10. Photograph (a) and sketch (b) of thrust faults in dolostone beds on the northwest limb.

the plunging axis parallel to the cut-off lines (i.e. line of intersection between the fault plane and bedding surface; Fig. 7e), which in turn coincides with the calculated fold axis (Fig. 2b). Block rotation and the resulting bookshelf geometry are accommodated by the ductile flow of shale into triangular-shaped pockets (Fig. 8a and b). Fourth, extensional fault length does not correlate with displacement (Fig. 9), and fifth, in some cases extensional faulting occurs along pre-existing oblique tectonic stylolites, providing an important temporal constraint.

In terms of localized strain, these faults accommodated a considerable amount of brittle extension in the three dolostone beds on the southeast limb. This extension occurred perpendicular to the fold axis, and thus was calculated in a line parallel to the bedding surface and normal to the fold axis, accounting for a degree of block rotation (calculated as the angle between bedding of the hanging wall block and overall non-rotated bedding) and an amount of dip separation. The scanlines were chosen along the limbs, not close to the hinge of the fold, in order to avoid changes in strain due to possible hinge migration. The strain was calculated as the sum of scanline-parallel extension determined for each fault, divided by the original scanline length. The magnitude of outer-arc extensional strain is 26% for bed #6 ($\Delta L = 11.2$ cm), 44% for bed #3 ($\Delta L = 4.6$ cm), and 26% for bed #1 ($\Delta L = 13.3$ cm), with the latter calculation including the sum of vein apertures ($\Delta L = 6.4$ cm). It should be noted that these estimates only refer to strain accommodated by brittle (i.e. fracture) deformation and do not include any component of ductile strain, and that the calculation represents a localized strain restricted to the region of faulting rather than a strain estimate for the entire southeast limb.

In contrast to the bed-confined faults in the dolostones, the other set of extensional faults extend across

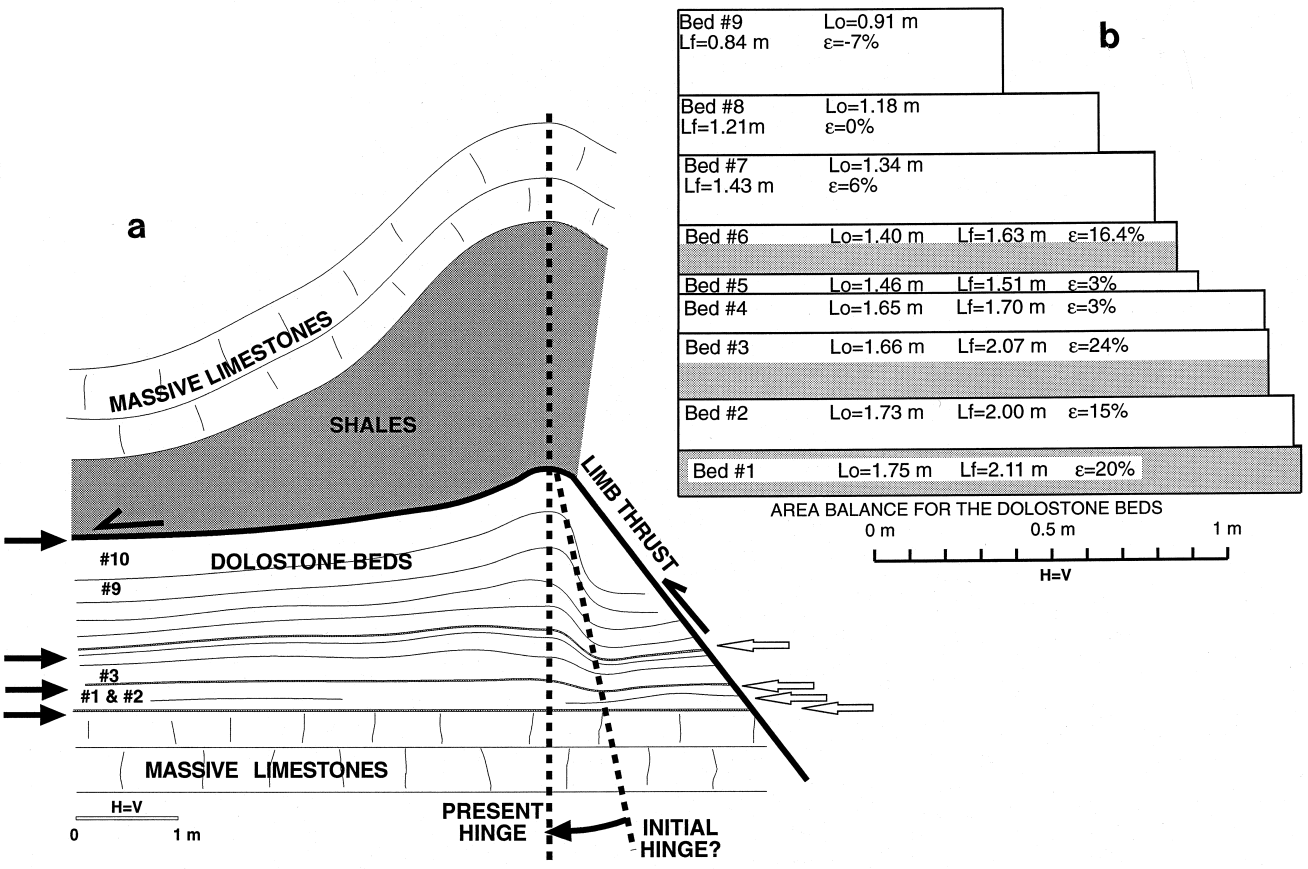

Fig. 11. (a) Reconstruction of bedding in dolostone section upon removal of limb dips. Note dramatic structural thinning of dolostone beds on the southeast limb, as well as key bedding-parallel slip horizons. Black arrows point to bed-parallel slip planes that operate during TLS. White arrows point to bed-parallel slip planes that operated to offset limb thrust. (b) Results of area balancing for each dolostone bed, including original length (L_0), final length (L_f) and strain (ε). Note the systematic decrease in extensional strain for packages of dolostone beds, and the presence of extensional faults (grey areas) on the outer arcs.

several beds in the upper bioclastic limestones (Fig. 8a). These four faults display a curved geometry with an ~20° counter-clockwise hanging wall block rotation around the plunging fold axis, opposite to the sense of rotation observed in the dolostones. Nevertheless, antithetically rotated blocks (e.g. Jordan, 1991) in the bioclastic limestones also accommodated axis-normal extension, as their cut-off lines are aligned with the calculated fold axis, and fault poles fall along the great circle normal to the fold axis (Fig. 7f). Dip separations range from 4 to 36 cm, although the number of faults were deemed too few to merit a strain calculation. Another important feature to note is that extensional faults close to the hinge zone displace previously-formed thrust duplexes.

3.3. Thrust faults

In marked contrast to the extensional faults observed on the southeast limb, the most prominent mesostructures on the northwest limb are contractional thrusts aligned at low angles to bedding (Figs. 5, 6 and 10). The thrusts are characterized by a flat geometry along bedding surfaces and a ramp geometry as they cut across dolostone beds, and are often aligned in a series of duplexes. Despite some scatter in orientation, the thrusts group into two conjugate sets, with the mean cut-off line approximately parallel to the fold axis (Fig. 7g). Some thrusts are confined to individual dolostone beds such as those found in beds #6, #7, #8, and #9. However, other thrusts cut across a mechanical unit consisting of several beds. In this case, beds #3, #4, and #5 act as a single mechanical unit, bounded above and below by thin shales which serve as floor and roof thrusts. The subparallel, low-angle thrusts form a duplex structure in between the bedding plane slip zones similar to structures reported by Tanner (1992).

The magnitude of shortening accommodated by thrusting on the northwest limb was estimated by removing displacement across the faults in each mechanical unit according to standard cross-section balancing techniques (Dahlstrom, 1969). In this manner we calculated a decrease in bed length of ~75 cm for each

bed ($\Delta L = -75$ cm), which corresponds to a bulk thrust-related shortening of 25% for the northwest limb. Two additional observations regarding the mesothrusts are noteworthy. First, thrust faults offset bed-normal stylolites (Figs. 6 and 10). Secondly, thrusts are not entirely restricted to the northwest limb; rather, thrust duplexes also appear in the hinge zone and even extend for limited distances into the southeast limb, most notably in beds #3, #8, and #9. As noted earlier, some of these thrusts on the southeast limb of the hinge zone were offset by extensional faults.

3.4. Limb thrust

The largest and most prominent mesostructure in the Bárzana fold is a subhorizontal to shallow-dipping thrust fault that transects the bioclastic limestone and dolostone units on the southeast limb (i.e. limb thrust of Ramsay and Huber, 1987) and intersects the overlying shale in the hinge zone. The fault, which transports the hanging wall to the northwest, strikes parallel to the fold axis trend and dips down plunge (Fig. 7h), with a maximum offset of ~2 m. Collapse of the hinge zone is accomplished by the thrust detaching along the shale–dolostone bed #10 contact upon intersecting the northwest limb, marking the transition from a ramp on ramp (southeast) to a flat on flat (northwest) geometry (Figs. 4–6). The fault consists of one main segment (thick line in Fig. 6) and one minor segment (thin line) that intersect in the hinge zone at the shale–dolostone bed #10 contact. The main segment has been deformed into a non-planar surface, resulting in a staircase geometry characterized by alternating shallow-dipping and steeply-dipping sections, the latter shorter in length and corresponding to bedding surfaces (Fig. 6). This unique geometry, first described by Watterson et al. (1998), results in a bimodal distribution of fault surface orientations (Fig. 7h), and indicates that the main thrust segment was deformed by bedding plane slip in the southeast limb. The undeformed smaller segment extends a limited distance from the branch line to its termination near the top of dolostone bed #2, and records a maximum offset of 12 cm.

In both the hanging wall and footwall, strata adjacent to the main thrust are locally dragged in the direction of opposing fault block motion (Fig. 6). As a result, small (~20 cm wavelength) drag folds developed in the interbedded carbonates and shales, whose hinges are aligned approximately parallel to the calculated fold axis (Fig. 7i). The orientation and sense of transport of the limb thrust as well as the orientation of thrust-related drag hinges indicate that the prominent thrust fault propagated in conjunction with overall fold development.

3.5. Area balance and bulk strain estimates for individual beds on the southeast limb

We performed a simple area balance for each bed in the dolostone unit on the southeast limb in order to estimate the total finite strain (we did not perform this analysis on the northwest limb because shortening on the northwest limb was uniform among all beds). An area balance for each bed is required due to the pronounced structural thickening and thinning of the strata, which invalidates the assumption of constant line length. To this end we unfolded the strata by rotating the limbs to their initial horizontal positions, while maintaining current bed thicknesses. The resulting two-dimensional cross-sectional profile (Fig. 11a) was constructed on the basis of seven detailed stratigraphical sections measured at different structural positions around the fold. The restoration demonstrates the dramatic thinning of the dolostone beds on the southeast limb, and the significant thickening of these beds in the hinge zone relative to both limbs (Fig. 11a). The sharp decrease in bed thickness on the southeast limb may indicate the approximate location of the original axial trace, which marked the early boundary between contractional structures on the northwest limb and extensional structures on the southeast limb. The contractional structures situated between the initial and present axial traces were subsequently extended during hinge migration. Also note the cut-off angle in the footwall of the limb thrust, which corresponds to systematically decreasing original bed lengths up-section, as well as the presence of thin shale beds that serve as key slip horizons (arrows).

The current length (i.e. final length) and thickness of each bed on the southeast limb was measured in order to compute cross-sectional area. A new rectangle of equal area was then drawn with one dimension equal to the true stratigraphic bed thickness (measured away from the fold in undeformed strata), and the other side therefore equal to the original bed length. Bulk strain was determined as the change in length divided by the original bed length. For the purpose of calculating finite strain we defined the boundary between limbs according to the present axial surface because (i) this defines the present boundary between contraction and extension, and (ii) the position of the initial hinge is not well-constrained, and its position would be assumed arbitrary. Consequently, the strain calculations may slightly underestimate extension because a small portion of the southeast limb (i.e. the area between the initial and present hinges) was structurally thickened prior to being extended.

Magnitudes of strain calculated for beds on the southeast limb are highly variable and range from 24% extension in bed #3 ($\Delta L = 41$ cm) to 7% contraction in bed #9 ($\Delta L = -5$ cm) (Fig. 11b). Despite such

heterogeneity, several important systematic trends in strain may be observed. The overall trend for the entire dolostone unit indicates a general decrease in extensional strain from the outer arc to the inner arc. Upon closer inspection, the dolostone beds are grouped into three separate packages of beds, each sandwiched between shale detachments. Within each package, the magnitude of extension systematically decreases from a maximum in the outer bed to a minimum in the inner bed. For example, bed #1 ($\Delta L = 36$ cm) and bed #2 ($\Delta L = 27$ cm) form one group of beds, with extensional strains of 20 and 15%, respectively. The middle dolostone package consists of beds #3 ($\Delta L = 41$ cm), #4 ($\Delta L = 5$ cm), and #5 ($\Delta L = 5$ cm), which record strains of 24, 3 and 3%, respectively. This pattern of strain indicates that each package of dolostone beds behaved as a rigid beam subjected to tangential longitudinal strain. Non-coincidentally, the outer bed in each group of dolostone beds (beds #1, #3, and #6) is in contact with a shale slip horizon and contains the prominent extensional faults described earlier (shaded grey in Fig. 11b).

Area balancing attests to a significant amount of internal (ductile) strain not apparent from observations of mesostructures. As opposed to the local fracture-related strains calculated from faults and veins, the estimates derived from area balancing provide a bulk strain (ductile and brittle) for the entire length of the southeast limb.

4. Discussion

The abundant and diverse collection of mesostructures provide the basis for unravelling the complex multi-stage folding process that occurred at Bárzana. Prior to constructing a model for fold development, we analyse the implications of the observed structural geometries. Of particular significance are the spatial distribution of mesostructures, temporal relations, angular relations, and effects of mechanical stratigraphy.

4.1. Analysis and interpretation of mesostructures and fold geometry

Tectonic stylolites provide a critical constraint on fold development. Two possible scenarios may explain the present geometry of the observed subvertical, bed-normal stylolites on the northwest limb and inclined, bed-oblique stylolites on the southeast limb. One possibility is that the two non-parallel sets of stylolites developed at different times in response to differently oriented axes of shortening. This is highly unlikely because it would require a noncoaxially inclined axis of regional shortening, and does not account for the divergence in stylolite orientation as a function of structural position with respect to the fold hinge. A more likely scenario is that the two sets of stylolites formed at the same time and were thus originally parallel to each other (Fig. 3), with the present difference in inclination arising from subsequent rotation of the southeast limb during fold tightening. Rotating the southeast limb back to the point where the tectonic stylolites on both limbs are parallel to each other yields the possible fold geometry at the onset of pressure solution. In this configuration, pressure solution occurs throughout the fold in response to northwest–southeast layer-parallel shortening, and local strain ellipses depicting pure shear shortening on each limb are similar to the regional deformation pattern. Not only does this explain the perpendicular vs oblique angular configurations with respect to bedding on opposing limbs, but it also demonstrates that tectonic stylolites developed after fold initiation. In fact, based on mean stylolite and bedding orientations, one can determine the dip of the southeast limb during the pressure solution phase, which was $\sim 60^\circ$. Non-coincidentally, this corresponds exactly to the proposed locking angle beyond which the flexural slip mechanism ceases to operate (Ramsay, 1967, 1974; Behzadi and Dubey, 1980). Thus, in all likelihood initial folding was accommodated by flexural slip. However, when the southeast limb reached a dip of 60° the bedding plane slip surfaces locked, requiring a switch in mechanism to pressure solution and hence the development of tectonic stylolites.

The preceding analysis of stylolite formation with respect to folding is based on the assumption that tectonic stylolites did not undergo internal rotation with respect to bedding. This assumption is valid because: (i) volume loss due to pressure solution is very small, and would result in negligible ($< 2^\circ$) changes in angular relations; (ii) stylolites are restricted to competent beds that deformed mostly by TLS; the bookshelf structures are restricted to outer arcs of the competent beds and formed in response to simple shear along bed boundaries, however the entire bed was not subjected to internal simple shear; and (3) the angle between tectonic stylolites and bedding is relatively uniform, regardless of the orientation of local bedding on the southeast limb.

Alignment of poles to extensional faults along the great circle normal to the fold axis (Fig. 7c), as well as the correspondence between fault cut-off lines and the fold axis (Fig. 7e–g) imply that fault development is directly related to the folding process. Faulting occurred after the phase of pressure solution, because tectonic stylolites on both limbs are displaced and/or reactivated. The correlation between the type of mesofault (i.e. thrust vs extensional) and structural position (i.e. northwest vs southeast limb) in a general sense is

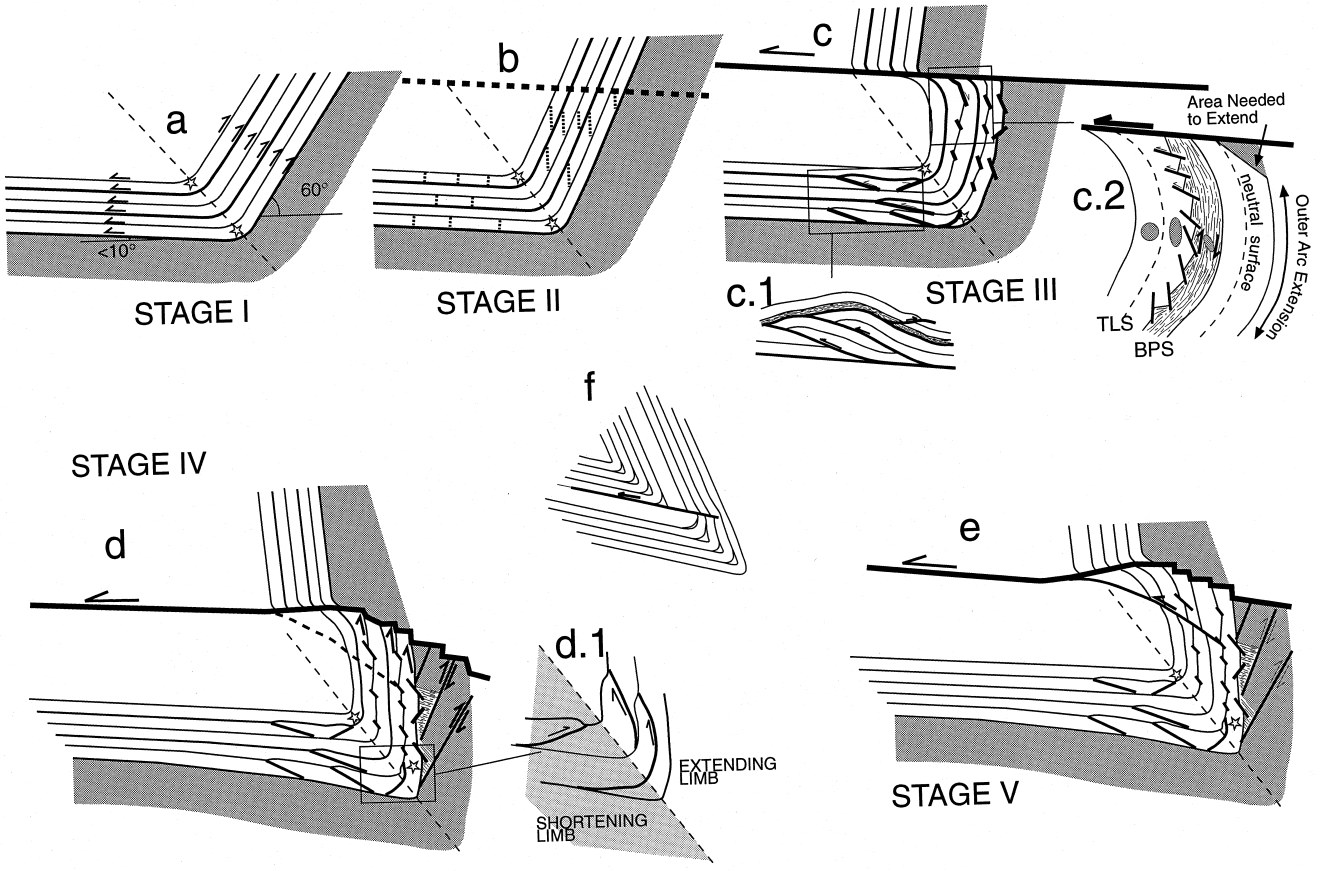

Fig. 12. Stages of fold development at Bárzana. Asterisks are reference points in dolostone beds along the original hinge line, and their movement into the southeast limb depicts hinge migration. (a) Stage I—Initial phase of flexural slip. (b) Stage II—Pressure solution and development of tectonic stylolites upon termination of flexural slip. (c) Stage III—Propagation of main limb thrust, bending of southeast limb, and mechanically-confined faulting in dolostone beds with thrusts on northwest limb and extensional faults on southeast limb. (d) Stage IV—Unlocking of bedding faults and resumption of flexural slip, resulting in deformation of main thrust and hinge migration. Extensional faulting in underlying limestones displace thrusts that passed through the hinge. (e) Stage V—Propagation of new limb thrust segment due to locking of main thrust. (f) Limb thrust adapted from Ramsay (1974).

a function of the angular relationship between limb dip and the regional strain ellipse; thrusts will shorten a subhorizontal limb because the axis of maximum shortening is parallel to bedding, whereas extensional faults will extend a subvertical limb because these strata are parallel to the axis of maximum extension (see fig. 2.14 of Ramsay and Huber, 1983). However, both the distribution and style of faulting on the southeast limb imply a mechanism more complex than passive limb rotation due to pure shear shortening. As opposed to the uniform ~25% shortening recorded by thrust faults in dolostones of the northwest limb, the magnitude of strain on the southeast limb varies dramatically as a function of mechanical stratigraphy and structural position. Growth of extensional faults from outer arcs to inner arcs of dolostone and their consistent terminations at neutral surfaces attest to the flexure of dolostone beds under tangential longitudinal strain. TLS is further supported by bulk strain estimates derived from area balancing, which reveal systematic decreases in strain for packages of beds between shale detachments.

The bookshelf geometry of extensional faults on the southeast limb implies the occurrence of simple shear in interbedded shales coeval with TLS in dolostones. The lack of correlation between displacement and length of extensional faults (Fig. 9) is further proof that the shales acted as detachments during fault growth (Gross et al., 1997b). Therefore, fold mechanism not only varied from one limb to the next during this stage, but also varied as a function of lithology within the southeast limb. Evidence for tangential longitudinal strain, in turn, indicates that the southeast limb underwent bending, perhaps due to propagation and displacement along the main limb thrust, and/or the curved fold shape imposed by the underlying massive limestones. Superimposed on bending of the southeast limb is a significant component of limb-parallel extension, as demonstrated by the magnitudes of bulk extensional strain.

Different mechanisms and thus different structures on opposing limbs mean that the hinge served as a boundary between structural domains. Thus, the presence of thrust duplexes southeast of the present axial surface implies a component of hinge migration away from the main limb thrust; small thrusts that originally developed on the northwest limb are now situated on the southeast limb. These duplexes were subsequently displaced by extensional faults upon reaching the southeast limb, although the precise timing of the relationship between hinge migration and extensional faulting on the southeast limb cannot be determined because the bioclastic limestone is not exposed in the hinge zone. The upward deflection of the main limb thrust (Figs. 4 and 6) provides further support for hinge migration, because it requires lengthening of the southeast limb as dolostone beds slipped past each other to create the staircase geometry.

4.2. Stages of Bárzana fold development

The described mesostructures, geometries, and temporal relationships provide the basis for our model of fold development at Bárzana. All structural data observed at the outcrop support a progressive coaxial deformation comprised of a temporally constrained sequence of folding stages. The model is depicted by schematically showing the mesostructural development through a series of stages (Fig. 12); for purposes of simplicity we ignore the fold plunge in our discussion of limb dips. The model begins with unfolded strata. Although studies have shown that a phase of layer-parallel shortening (e.g. cleavage development, internal finite strain) often precedes folding in detachment-related fold and thrust belts (e.g. Engelder and Engelder, 1977; Geiser and Engelder, 1983; Gutiérrez-Alonso and Gross, 1997), we did not observe any evidence for pre-folding finite strain in the outcrop. The initial stage (I) of deformation resulted in the development of locally west-verging asymmetric folds (Fig. 12a), and was accommodated by the flexural slip mechanism as manifested by numerous dip-slip lineations on bedding plane faults and other kinematic criteria (Figs. 2d and 3). Slip was concentrated along discrete shale horizons while dolostone beds maintained their uniform orthogonal thicknesses, resulting in a parallel (Class 1B) geometry for the dolostone unit. The overlying shale flowed from the limbs and into the hinge zone. The flexural slip mechanism prevailed until the southeast limb reached a dip of $\sim 60^{\circ}$, at which point the slip surfaces locked.

The termination of flexural slip required the initiation of a new mechanism to accommodate further fold development. Thus began the phase of pressure solution (stage II), whereby tectonic stylolites developed on both limbs. The stylolites originated as subvertical surfaces, parallel to each other on opposite limbs in response to continued subhorizontal northwest–southeast shortening (Figs. 3 and 12b). However, because the strata were already folded prior to pressure solution, the angle between stylolite and bedding surfaces differed: bed-normal stylolites developed on the northwest limb while stylolites on the southeast limb grew oblique to bedding. During the phase of pressure solution the strata were tectonically shortened and the southeast limb may have passively rotated by several degrees; however, the relatively wide stylolite spacing and low seam amplitude suggest that this phase was relatively short-lived.

Intensification of northwest-directed shortening required a switch to other mechanisms to accommodate greater amounts of strain. The next folding phase (stage III) resulted in the development of mesofaults and the main limb thrust, though their relative timing with respect to each other is unclear (Fig. 12c). The southeast limb was simultaneously bent and stretched, with the strain accommodated by a combination of extensional faulting, veining and internal ductile deformation. Dolostone beds were subjected to tangential longitudinal strain while simple shear occurred within intervening shale horizons, resulting in the observed bookshelf geometry for extensional faults that propagated from outer arcs of dolostone packages. While bending predominated in the southeast limb, thrust faults developed in the northwest limb in response to pure shear shortening. Thrust faults displaced pre-existing tectonic stylolites on the northwest limb while several oblique tectonic stylolites were reactivated as extensional faults on the southeast limb. Displacement and drag along the main thrust in part may have been responsible for generating the bending and stretching forces in the southeast limb. This phase of fold development led to thickening of the northwest limb and hinge zone and dramatic thinning of the southeast limb (Fig. 11) and hence marked a deviation from the parallel fold geometry that persisted in the dolostone unit during the earlier flexural slip phase.

Thickening of the overlying shale in the hinge zone during early stages of folding may have facilitated detachment of the limb thrust as it propagated westward into the synclinal core. In any case, development of the main thrust ultimately unlocked the bedding plane slip surfaces so that continued fold tightening resulted in their reactivation. Thus began a second phase of bedding plane slip (stage IV) whereby dip-slip motion along bedding plane faults offset the hinge parallel veins that formed under TLS (Fig. 3b), faulted the underlying bioclastic limestones, and deformed the main thrust into its unique staircase geometry (Fig. 12d). Geometrical modelling indicates that hinge migration occurred during this phase as part of the northwest limb was pulled into the southeast limb.

Consequently, several thrusts that originated on the northwest limb are now found on the southeast limb. Displacement of the main thrust by renewed flexural slip, in turn, effectively precluded it from accommodating further displacement. Consequently, a new thrust segment developed beneath the main thrust. This is the younger fault segment representing the most recent phase of fold-related deformation (stage V) because it has not been offset by bedding plane slip (Fig. 12e), and effectively widens the fault zone in the manner described by Watterson et al. (1998).

4.3. Relation to current fold models

As described above, fold mechanisms that operated during development of the Bárzana syncline include two separate phases of flexural slip, layer-parallel shortening accompanied by pressure solution, tangential longitudinal strain, and hinge collapse accommodated by a limb thrust. We now attempt to place the structural development within the context of current folding models—fault-propagation folds, trishear fault-propagation folds, and break thrust folds. In a fault-propagation fold, the fold develops in advance of and in response to a propagating thrust fault (Suppe, 1985). The Bárzana fold, however, developed prior to the thrust that transects the southeast limb. In fact, thrusting was a direct consequence of fold development (i.e. a 'a fold-related thrust'), and was the mechanism that enabled progressive fold tightening subsequent to locking of the bedding plane faults. The southeast termination of the limb thrust is situated in the middle of the southeast limb, and does not merge into a larger fault or detachment at lower structural levels (Fig. 2). A fault of such limited dimension and slip cannot create the Bárzana-scale fold. Consequently, the trishear model for fault-propagation folding (Erslev, 1991; Hardy and Ford, 1997; Allmendinger, 1998) is not applicable, although the mesostructures observed on both limbs represent a zone of distributed strain, albeit non-triangular in shape.

The models that best describe the Bárzana fold in terms of geometry and progressive development are the 'limb thrust' (Ramsay, 1974; Ramsay and Huber, 1987) and the 'break thrust' (Willis, 1893; Fischer et al., 1992). Both models invoke an early phase of fold amplification that terminates upon locking of bedding plane faults. Subsequent shortening occurs by development of a thrust that transects one of the limbs. Although the strict definition of a break thrust describes a thrusted fold limb (Willis, 1893), current models genetically relate break thrusts to fault-related folding, with emphasis on fixed-hinge buckling (Fischer et al., 1992). The Bárzana structure is a fold-related thrust, thus the limb thrust of Ramsay (1974) is the most appropriate current model because the thrust is restricted to an individual fold, and forms in response to space problems and tightening difficulties encountered by that fold. Note the similarity between the Bárzana thrust and Ramsay's limb thrust (Fig. 12f), especially the transection of competent beds in the limb and the detachment within the thickened incompetent beds in the core.

5. Conclusions

Several important implications arise from analysis of the Bárzana fold. First, it may be unreasonable to assume the operation of a single fold mechanism throughout the history of fold development, especially for tight, overturned, and faulted folds. This study demonstrates that the folding process switches to new mechanisms when older mechanisms are no longer able to accommodate further tightening and changes in fold geometry. Not only can the mechanism vary through time, but it also can vary as a function of structural position. For example, while the northwest limb experienced homogeneous pure shear shortening, the southeast limb was subjected to a combination of tangential longitudinal strain in dolostones and simple shear in interbedded shales due to applied bending forces. Although the Bárzana fold likely developed in response to uniformly-oriented subhorizontal northwest–southeast regional contraction, operating mechanisms on a local scale include two separate phases of flexural slip, pressure solution, thinning and thickening of opposing limbs, and the propagation of a limb thrust that led to hinge collapse.

Secondly, careful analysis of mesostructures provides the criteria for unravelling the complex history of fold development at Bárzana. For example, the two sets of tectonic stylolites on opposite limbs were used to determine the locking angle of early-phase flexural slip, and provide the fold geometry at the onset of pressure solution. Furthermore, when flexural slip ceases to operate, continued folding may lead to dramatic changes in bed thicknesses. Thus, the assumption that beds maintain uniform thickness must be revisited when balancing cross-sections in tightly folded terranes. Alignment of extensional faults as bookshelves attests to the important role played by mechanical stratigraphy, whereby structural style is controlled to a large extent by contrasts in lithology. While flexural slip surfaces may lock once critical limb dips or interlimb angles are reached, propagation of a fault across the limb may unlock these faults and thus permit their subsequent reactivation.

Third, bending and stretching of the southeast limb led to intense localized fracture-related strain in the form of hinge-parallel extension faults and veins.

Limbs of footwall synclines are considered important hydrocarbon traps in fold and thrust belts. Our study suggests that competent beds in these limbs may be intensely fractured, and hence may represent excellent fractured reservoir targets as a result of the folding and faulting processes described in this paper.

Acknowledgements

We benefited from discussions with Juan Luis Alonso, Fernando Bastida, and Mark P. Fischer. Funding for this project was provided by a NATO Collaborative Research Grant (CRG 951350) awarded to the authors by the Assistant Secretary General for Scientific and Environmental Affairs. Additional funding for GGA was provided by Education and Culture Ministry project PB96-1452-CO-03-02. We thank Ken McClay and Mike Coward for their helpful reviews.

References

Allmendinger, R.W., 1998. Inverse and forward numerical modeling of trishear fault-propagation folds. Tectonics 17, 640–656.

Alonso, J.L., Aller, J., Bastida, F., Marcos, A., Marquinez, J., Pérez-Estaún, A., Pulgar, J.A., 1991. Mapa geológico y memoria Nº 2 (Avilés). Instituto Tecnológico Geominero de España, scale 1:200,000.

Bastida, F., Castro, S., 1988. Estructura del sector septentrional de la Escama de Tameza (Zona Cantábrica, NW de España). Trabajos de Geología Universidad de Oviedo 17, 67–85.

Bastida, F., Gutiérrez-Alonso, G., 1989. Síntesis cartográfica de las unidades occidentales de la Zona Cantábrica. Trabajos de Geología Universidad de Oviedo 18, 117–125.

Bastida, F., Marcos, A., Pérez-Estaún, A., Pulgar, J.A., 1984. Geometría y evolución estructural del Manto de Somiedo (Zona Cantábrica, NO de España). Boletín Instituto Geológico y Minero de España 95, 517–539.

Becker, A., Mazor, E., Becker, N., 1995. Flexural slip in an anticlinal plungeout as a mechanism for dike offsets: Nahal Ardon Valley, Ramon National Geological Park, Israel. International Geology Review 37, 601–622.

Behzadi, H., Dubey, A.K., 1980. Variation of interlayer slip in space and time during flexural folding. Journal of Structural Geology 2, 453–457.

Chapple, W.M., Spang, J.H., 1974. Significance of layer-parallel slip during folding of layered sedimentary rocks. Geological Society of America Bulletin 85, 1523–1534.

Choukroune, P., 1969. Un exemple d'analyse microtectonique d'une series calcaire affectee de plis isopaque ('concentrique'). Tectonophysics 7, 57–70.

Crespo Zamorano, A., 1982. Mapa Geológico de España, 2ª Serie. Hoja nº 76 (Pola de Somiedo). Instituto Geológico y Minero de España, scale 1:50,000.

Dahlstrom, C.D.A., 1969. Balanced cross sections. Canadian Journal of Earth Sciences 6, 743–757.

de Sitter, L.U., 1958. Boudins and parasitic folds in relation to cleavage and folding. Geologie Minjbon 20, 277–288.

Engelder, T., Engelder, R., 1977. Fossil distortion and decollement tectonics on the Appalachian Plateau. Geology 5, 457–460.

Erslev, E.A., 1991. Trishear fault-propagation folding. Geology 19, 617–620.

Eyal, Y., Reches, Z., 1983. Tectonic analysis of the Dead Sea rift region since the Late-Cretaceous based on mesostructures. Tectonics 2, 167–185.

Fischer, M.P., Woodward, N.B., Mitchell, M.M., 1992. The kinematics of break-thrust folds. Journal of Structural Geology 14, 451–460.

Geiser, P.A., Engelder, T., 1983. The distribution of layer parallel shortening fabrics in the Appalachian foreland of New York and Pennsylvania: evidence for two non-coaxial phases of the Allghenian orogeny. In: Hatcher, R.D., Williams, H., Zeitz, I. (Eds.), Geological Society of America Memoir 158, pp. 161–175.

Gross, M.R., Fischer, M.P., Engelder, T., Greenfield, R.J., 1995. Factors controlling joint spacing in interbedded sedimentary rocks: integrating numerical models with field observations from the Monterey Formation, USA. In: Ameen, M.S. (Ed.), Fractography: Fracture Topography as a Tool in Fracture Mechanics and Stress Analysis, Geological Society Special Publication 192, 215–233.

Gross, M.R., Engelder, T., 1995. Strain accommodated by brittle failure in adjacent units of the Monterey formation, USA: scale effects and evidence for uniform displacement boundary conditions. Journal of Structural Geology 17, 1303–1318.

Gross, M.R., Becker, A., Gutiérrez-Alonso, G., 1997a. Transfer of displacement from multiple slip zones to a major detachment in an extensional regime: Example from the Dead Sea rift, Israel. Geological Society of America Bulletin 109, 1021–1035.

Gross, M.R., Gutiérrez-Alonso, G., Bai, T., Wacker, M.A., Collinsworth, K.B., Behl, R.J., 1997b. Influence of mechanical stratigraphy and kinematics on fault scaling relations. Journal of Structural Geology 19, 171–183.

Gutiérrez-Alonso, G., 1987. La estructura de la parte Norte de la Ventana Tectónica del Narcea (Zona Cantábrica, NW de España). Seminario de Investigación, Universidad de Oviedo, 42 pp.

Gutiérrez-Alonso, G., 1992. El Antiforme del Narcea y su relación con los mantos occidentales de la Zona Cantábrica. PhD thesis, University of Oviedo.

Gutiérrez-Alonso, G., 1996. Strain partitioning in the footwall of the Somiedo Nappe: structural evolution of the Narcea Tectonic Window, NW Spain. Journal of Structural Geology 18, 1217–1229.

Gutiérrez-Alonso, G., Gross, M.R., 1997. Geometry of inverted faults and related folds in the Monterey Formation: implications for the structural evolution of the southern Santa Maria Basin, California. Journal of Structural Geology 19, 1303–1321.

Hardy, S., Ford, M., 1997. Numerical modeling of trishear fault propagation folding. Tectonics 16, 841–854.

Heredia, N., 1984. La estructura de la escama de Villar de Vildas (Manto de Somiedo, Zona Cantábrica). Trabajos de Geología Universidad de Oviedo 14, 65–78.

Jordan, P.G., 1991. Development of asymmetric shale pull-aparts in evaporite shear zones. Journal of Structural Geology 13, 399–409.

Julivert, M., 1971. Decollement tectonics in the Hercynian Cordillera of NW Spain. American Journal of Science 270, 1–29.

Julivert, M., Pello, J., Fernandez, L., 1968. La estructura del Manto de Somiedo (Cordillera Cantábrica). Trabajos de Geología Universidad de Oviedo 2, 1–43.

Julivert, M., Marcos, A., Pulgar, J.A., 1977. Mapa Geológico de España 2ª Serie, Hoja nº 27 (Belmonte de Miranda). Instituto Geológico y Minero de España, scale 1:200,000.

Merino, E., 1992. Self-organization in stylolites. American Scientist 80, 466–473.

Merino, E., Ortoleva, P., Strickholm, P., 1983. Generation of evenly-spaced pressure-solution seams during (late) diagenesis: A kinetic theory. Contributions to Mineralogy and Petrology 82, 360–370.

Mitra, S., 1990. Fault-propagation folds: geometry, kinematics, and hydrocarbon traps. American Association of Petroleum Geologists Bulletin 74, 921–945.

Mitra, S., Namson, J.S., 1989. Equal-area balancing. American Journal of Science 289, 563–599.

Narr, W., Suppe, J., 1991. Joint spacing in sedimentary rocks. Journal of Structural Geology 13, 1037–1048.

Pérez-Estaún, A., Bastida, F., Alonso, J.L., Marquinez, J., Aller, J., Alvarez-Marrón, J., Marcos, A., Pulgar, J., 1988. A thin skinned tectonic model for an arcuate fold and thrust belt: The Cantabrian Zone (Variscan Iberoarmorican Arc). Tectonics 7, 517–537.

Pérez-Estaún, A., Martínez-Catalán, J.R., Bastida, F., 1991. Crustal thickening and deformation sequence in the footwall to the suture of the Variscan belt of northwest Spain. Tectonophysics 191, 243–253.

Pérez-Estaún, A., Pulgar, J.A., Banda, E., Alvarez-Marrón, J., 1994. Crustal structure of the external variscides in northwest Spain from deep seismic reflection profiling. Tectonophysics 232, 91–118 (also the ESCI-N Research Group).

Price, N.J., Cosgrove, J.W., 1990. Analysis of Geological Structures. Cambridge University Press, Cambridge.

Ramsay, J.G., 1967. Folding and Fracturing of Rocks. McGraw-Hill, New York.

Ramsay, J.G., 1974. Development of chevron folds. Geological Society of America Bulletin 85, 1741–1754.

Ramsay, J.G., Huber, M.I., 1983. In: The Techniques of Modern Structural Geology, Volume I: Strain Analysis. Academic Press, London.

Ramsay, J.G., Huber, M.I., 1987. In: The Techniques of Modern Structural Geology, Volume II: Folds and Fractures. Academic Press, London.

Schlische, R.W., Young, S.S., Ackermann, R.V., Gupta, A., 1996. Geometry and scaling relations of a population of very small rift-related normal faults. Geology 24, 683–686.

Suárez, A., Heredia, N., López, F., Toyos, J.M., Rodríguez Fernández, L.R., Gutiérrez Alonso, G., 1990. Mapa Geológico de España 2ª serie, Nº 102 (Barrios de Luna). Instituto Tecnológico Geominero de España, scale 1:50,000.

Suppe, J., 1983. Geometry and kinematics of fault bend folding. American Journal of Science 283, 684–721.

Suppe, J., 1985. Principles of Structural Geology. Prentice-Hall, Englewood Cliffs, New Jersey.

Tanner, P.W.G., 1989. The flexural-slip mechanism. Journal of Structural Geology 11 (6), 635–655.

Tanner, P.W.G., 1992. Morphology and geometry of duplexes formed during flexural-slip folding. Journal of Structural Geology 14, 1173–1192.

Twiss, R.J., Moores, E.M., 1992. Structural Geology. Freeman, New York.

Watterson, J., Childs, C., Walsh, J.J., 1998. Widening of fault zones by erosion of asperities formed by bed-parallel slip. Geology 26, 71–74.

Willis, B., 1893. Mechanics of Appalachian structure. U.S. Geological Survey Annual Report 13 (1891–1892), part 2, pp. 217–281.